View metadata, citation and similar papers at core.ac.uk

brought to you by CORE

provided by Tsukuba Repository

Spectroscopic evidence of photogenerated carrier separation by built-in electric field in Sb-doped n-BaSi2/B-doped p-BaSi2 homojunction diodes

著者	Kodama Komomo, Takabe Ryota, Deng Tianguo, Toko Kaoru, Suemasu Takashi
journal or publication title	Japanese Journal of Applied Physics
volume	57
number	5
page range	050310
year	2018-04
権利	(C) 2017 The Japan Society of Applied Physics Content from this work may be used under the terms of the Creative Commons Attribution 4.0 license . Any further distribution of this work must maintain attribution to the author(s) and the title of the work, journal citation and DOI.
URL	http://hdl.handle.net/2241/00151546

doi: 10.7567/JJAP.57.050310

Creative Commons : 表示
http://creativecommons.org/licenses/by/3.0/deed.ja

Japanese Journal of Applied Physics

The Japan Society of Applied Physics

RAPID COMMUNICATIONS • OPEN ACCESS

Spectroscopic evidence of photogenerated carrier separation by built-in electric field in Sb-doped n-$BaSi_2$/B-doped p-$BaSi_2$ homojunction diodes

To cite this article: Komomo Kodama *et al* 2018 *Jpn. J. Appl. Phys.* **57** 050310

View the article online for updates and enhancements.

Related content

- Decrease in electrical contact resistance of Sb-doped n^+-$BaSi_2$ layers and spectral response of an Sb-doped n^+-$BaSi_2$/undoped $BaSi_2$ structure for solar cells
  Komomo Kodama, Ryota Takabe, Suguru Yachi et al.
- Effect of p-$BaSi_2$ layer thickness on the solar cell performance of p-$BaSi_2$/n-Si heterojunction solar cells
  Suguru Yachi, Ryota Takabe, Kaoru Toko et al.
- Growth of $BaSi_2$ continuous films on Ge(111) by molecular beam epitaxy and fabrication of p-$BaSi_2$/n-Ge heterojunction solar cells
  Ryota Takabe, Suguru Yachi, Daichi Tsukahara et al.

This content was downloaded from IP address 130.158.56.92 on 01/05/2018 at 02:11

OPEN ACCESS

Japanese Journal of Applied Physics **57**, 050310 (2018)

https://doi.org/10.7567/JJAP.57.050310

RAPID COMMUNICATION

Spectroscopic evidence of photogenerated carrier separation by built-in electric field in Sb-doped n-$BaSi_2$/B-doped p-$BaSi_2$ homojunction diodes

Komomo Kodama, Ryota Takabe, Tianguo Deng, Kaoru Toko, and Takashi Suemasu*

Institute of Applied Physics, Graduate School of Pure and Applied Sciences, University of Tsukuba, Tsukuba, Ibaraki 305-8573, Japan

*E-mail: suemasu@bk.tsukuba.ac.jp

Received February 24, 2018; accepted March 14, 2018; published online April 16, 2018

The operation of a $BaSi_2$ homojunction solar cell is first demonstrated. In n^+-$BaSi_2$ (20 nm)/p-$BaSi_2$ (500 nm)/p^+-$BaSi_2$ (50 nm) homojunction diodes on p^+-Si(111) (resistivity $\rho < 0.01\,\Omega\,cm$), the internal quantum efficiency (*IQE*) under AM1.5 illumination becomes pronounced at wavelengths $\lambda < 800$ nm and exceeded 30% at $\lambda = 500$ nm. In contrast, the *IQE* values are small at $\lambda < 600$ nm in n^+-$BaSi_2$ (300 nm)/p-Si ($\rho > 0.1\,\Omega\,cm$) heterojunction diodes, but are high in the range between 600 and 1200 nm. The difference in spectral response demonstrates the photogenerated carrier separation by the built-in electric field in the homojunction diode. © 2018 The Japan Society of Applied Physics

The conversion efficiency (η) of crystalline Si (c-Si) solar cells has exceeded 26%,[1] and is now approaching the theoretical efficiency limit.[2] Therefore, alternative solar cell materials are being examined, including III–V semiconductors, chalcopyrites, CdTe, and perovskites.[3–7] A large absorption coefficient (α), a suitable band gap, and superior minority-carrier properties are important for solar cell materials to achieve a high η. Among such materials, we have focused on semiconducting barium disilicide ($BaSi_2$).[8,9] This is because $BaSi_2$ has all these properties such as a band gap of 1.3 eV,[10] a large α of $3 \times 10^4\,cm^{-1}$ at 1.5 eV,[10–13] inactive grain boundaries,[14] and a large minority-carrier lifetime ($\tau \sim 10\,\mu s$).[15,16] Since $BaSi_2$ can be grown epitaxially on a Si substrate[17] and its band gap can be increased by adding other elements such as Sr and C,[18,19] $BaSi_2$ is a material of choice for targeting $\eta > 30\%$ in a Si-based tandem structure solar cell. As a first step, we chose a p-$BaSi_2$/n-Si heterojunction structure and have achieved η approaching 10%.[20,21] This is the highest η ever recorded for solar cells fabricated with semiconducting silicides. Our next target is to achieve a high η in a $BaSi_2$ homojunction solar cell towards tandem solar cells. However, there has been no report thus far on the demonstration of a $BaSi_2$ homojunction solar cell. It is important to mention that since the band gap of Si is smaller than that of $BaSi_2$, photogenerated carriers originating from the Si substrate inevitably contribute to the spectral response of a $BaSi_2$ homojunction diode formed on Si. This makes it difficult to verify the operation of the $BaSi_2$ homojunction solar cell. One way to avoid this problem is to make use of heavily doped Si substrates having a small minority-carrier lifetime. According to our previous work,[22] however, step bunching occurs to a far greater extent when a heavily doped (low resistivity $\rho < 0.01\,\Omega\,cm$) Si substrate is heated at 900 °C for 30 min in an ultrahigh-vacuum chamber to remove the protective oxide layer on the surface. Step bunching causes the generation of defects around the $BaSi_2$/Si heterointerface.[22] Actually, such low-ρ Si substrates are not available in a $BaSi_2$-pn/Si-pn tandem structure solar cell. Thereby, we put emphasis of this article not on the η but on the demonstration of a $BaSi_2$ homojunction solar cell from the viewpoint of spectral response. As the topmost layer of a $BaSi_2$ homojunction solar cell, we chose an Sb-doped n-$BaSi_2$ layer instead of a B-doped p-$BaSi_2$ layer because the contact resistance of Al/Sb-doped n-$BaSi_2$ was much smaller than that of Al/B-doped p-$BaSi_2$.[23]

We used an ion-pumped molecular beam epitaxy (MBE) system equipped with an electron-beam evaporation source for 10N-Si as well as standard Knudsen cells for 3N-B, 5N-Sb, and 3N-Ba. Details of the growth procedure of Sb-doped n-$BaSi_2$ and B-doped p-$BaSi_2$ were reported previously.[20,23] To find the growth condition for heavily Sb-doped n-$BaSi_2$, we used high-ρ p-Si(111) substrates ($\rho > 10^3\,\Omega\,cm$). After thermally cleaning the substrate at the substrate temperature $T_S = 900$ °C, we deposited Ba at $T_S = 500$ °C to form a 5-nm-thick $BaSi_2$ template layer by reactive deposition epitaxy. This template worked as seeds that control the crystal orientation of the $BaSi_2$ overlayers.[24] Next, we grew 300-nm-thick Sb-doped n-$BaSi_2$ epitaxial layers by MBE with varying T_S values of 500, 540, and 580 °C. The electron concentration n of Sb-doped n-$BaSi_2$ depends on T_S.[25] Then, a 3-nm-thick amorphous Si (a-Si) layer was in situ deposited at $T_S =$ 180 °C to prevent surface oxidation.[26] Ohmic contacts were formed with Al by sputtering. Carrier concentration and mobility were measured by the van der Pauw method. The depth profile of Sb atoms was measured by secondary ion mass spectrometry (SIMS) using Cs^+ ions.

We next formed two types of pn junction diodes, namely, n^+-$BaSi_2$ (300 nm)/p-Si heterojunction diodes on medium-doped p-Si(111) ($\rho > 0.1\,\Omega\,cm$), and n^+-$BaSi_2$ (20 nm)/p-$BaSi_2$ (500 nm)/p^+-$BaSi_2$ (50 nm) homojunction diodes on heavily doped p^+-Si(111) ($\rho < 0.01\,\Omega\,cm$). All the $BaSi_2$ surfaces were in situ capped with a 3-nm-thick a-Si layer.[27] In both cases, we chose T_S at 500 °C for n^+-$BaSi_2$ and fixed its n value at approximately $2 \times 10^{19}\,cm^{-3}$. In the homojunction diode, we set the hole concentration p of the p^+-$BaSi_2$ (50 nm) layer at approximately $1 \times 10^{19}\,cm^{-3}$. This is to obtain a good electrical contact for a hole transport across the p^+-$BaSi_2$ (50 nm)/p^+-Si interface to overcome a large valence band offset ($\Delta E_V \sim 0.6$ eV) caused by a small electron affinity of $BaSi_2$ (3.2 eV).[28] Regarding the 500-nm-thick p-$BaSi_2$ layer, we varied the p value as 1×10^{16} or $1 \times 10^{17}\,cm^{-3}$. For optical characterization, an 80-nm-thick indium–tin-oxide electrode (diameter = 1 mm) was sputtered on the front side and a 150-nm-thick Al electrode was sputtered on the entire back side. The current density versus voltage (J–V) characteristics under standard AM1.5 illumination and the photoresponse spectra

Content from this work may be used under the terms of the Creative Commons Attribution 4.0 license. Any further distribution of this work must maintain attribution to the author(s) and the title of the work, journal citation and DOI.

© 2018 The Japan Society of Applied Physics

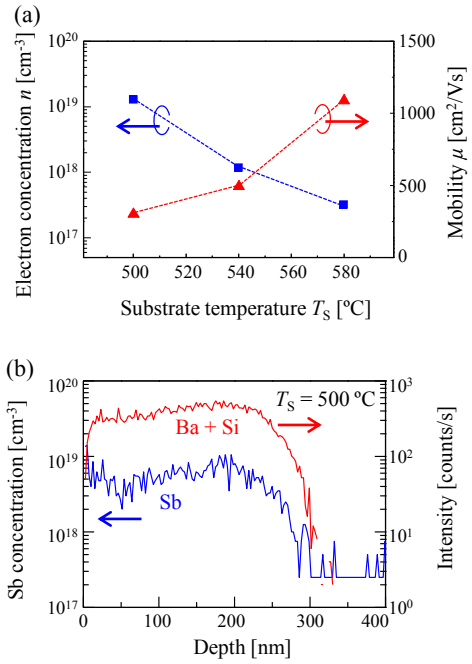

Fig. 1. (Color online) (a) Substrate temperature dependence of electron concentration and mobility for Sb-doped n-$BaSi_2$. (b) SIMS depth profile of Sb atoms and secondary ions (Ba + Si) for the sample grown at $T_S = 500$ °C.

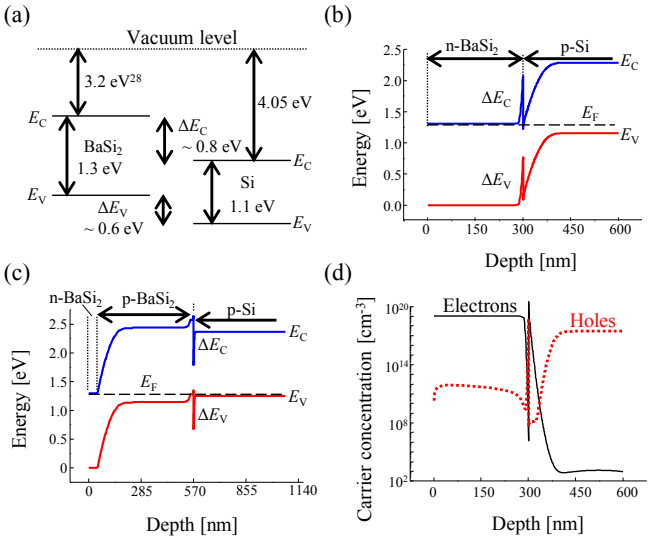

Fig. 2. (Color online) (a) Band alignment of $BaSi_2$ and Si with respect to the vacuum level. Calculated band alignments by AFORS-HET for (b) n$^+$-$BaSi_2$/p-Si and (c) n$^+$-$BaSi_2$/p-$BaSi_2$/p$^+$-$BaSi_2$/p$^+$-Si diodes. (d) Carrier concentration profiles in (a) at a forward bias voltage of 1.8 V.

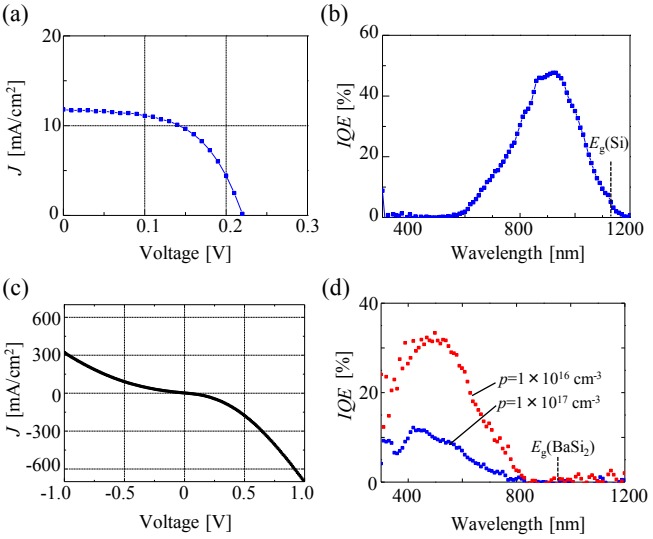

Fig. 3. (Color online) (a) J–V characteristics under AM1.5 illumination and (b) IQE spectrum for n$^+$-$BaSi_2$/p-Si and (c, d) those for n$^+$-$BaSi_2$/p-$BaSi_2$/p$^+$-$BaSi_2$/p$^+$-Si diodes. The wavelengths corresponding to the band gaps of Si and $BaSi_2$ are marked in (b) and (d), respectively.

were measured using a xenon lamp with a 25-cm-focal-length single monochromator (Bunko Keiki SM-1700A and RU-60N). The light intensity of the lamp was calibrated using a pyroelectric sensor (Melles Griot 13PEM001/J). Reflectance spectra were evaluated with a reflection measurement system using a xenon lamp with an integrating sphere. All measurements were performed at ambient temperature. The band alignment of the diodes and carrier concentration profile were simulated by automat for simulation of heterostructures (AFORS-HET),[29] where the ideal condition such as no defects was assumed.

Figure 1(a) shows n and mobility values of Sb-doped n-$BaSi_2$ films against T_S. n decreased with increasing T_S, owing to the large vapor pressure of Sb,[30] and reached approximately 10^{19} cm^{-3} at $T_S = 500$ °C. Because of this, $T_S = 500$ °C was fixed for the following pn diode investigations. The mobility decreased as n increased. This trend is usually predicted by ionized impurity scattering in conventional semiconductors. Figure 1(b) shows the SIMS depth profile of Sb atoms and secondary ions (Si + Ba) for the sample grown at $T_S = 500$ °C. The Sb atoms were relatively uniformly distributed in the grown layer. The Sb concentration was slightly smaller than the measured value ($n = 1.3 \times 10^{19}$ cm^{-3}). Both first-principles calculation and experiment revealed that the deviation of the Ba/Si atomic ratio in $BaSi_2$ from stoichiometry gives rise to electrons.[31,32] We suppose that is why the n value was higher than the Sb concentration.

Figure 2(a) shows the band alignment of $BaSi_2$ and Si with respect to the vacuum level, and Figs. 2(b) and 2(c) show the band alignments of n$^+$-$BaSi_2$ (300 nm, $n = 1 \times 10^{19}$ cm^{-3})/p-Si ($\rho > 0.1\,\Omega$ cm) and n$^+$-$BaSi_2$ (20 nm, $n = 1 \times 10^{19}$ cm^{-3})/p-$BaSi_2$ (500 nm, $p = 1 \times 10^{17}$ cm^{-3})/p$^+$-$BaSi_2$ (50 nm, $p = 1 \times 10^{19}$ cm^{-3})/p$^+$-Si(111) ($\rho < 0.01\,\Omega$ cm) diodes. In Fig. 2(b), the depletion region stretches mostly towards the p-Si side because of a large difference in impurity concentration. Figure 2(d) shows the band alignment of the diode when a forward bias voltage of 1.8 V, corresponding to the open-circuit voltage (V_{OC}), was applied. At the n$^+$-$BaSi_2$/p-Si heterointerface, there is a large conduction band offset ($E_C \sim 0.8$ eV) for photogenerated electrons in the p-Si substrate to travel to the n$^+$-$BaSi_2$ layer and a large ΔE_V for photogenerated holes in the n$^+$-$BaSi_2$ layer to be transferred into the p-Si substrate. Such large band offsets disturb the carrier transport of photogenerated carriers and hence they accumulate at the heterointerface as shown in Fig. 2(d). In Fig. 2(c), the influence of a large ΔE_V at the p$^+$-$BaSi_2$/p$^+$-Si was diminished by using the heavily doped p$^+$-Si substrate.

Figures 3(a) and 3(b) show typical examples of rectifying J–V characteristics under AM1.5 illumination and internal quantum efficiency (IQE) spectrum for the n$^+$-$BaSi_2$/p-Si diode. A short-circuit current density J_{SC} of 11.8 mA/cm^2, $V_{OC} = 0.22$ V, and $\eta = 1.5\%$ were obtained. The values of J_{SC},

© 2018 The Japan Society of Applied Physics

V_{OC}, and η are much smaller than those obtained in B-doped p-$BaSi_2$/n-Si heterojunction solar cells.[21] This is because the band offsets at the n^+-$BaSi_2$/p-Si interface hinder the transport of photogenerated carriers, promoting the recombination of accumulated electrons and holes via defects at the heterointerface as shown in Fig. 2(c). Actually, the reverse saturation current density of the diode (J_0) was calculated to be 2.4×10^{-2} mA/cm^2 by using a technique described in Ref. 33. This value is more than three orders of magnitude higher than that for B-doped p-$BaSi_2$/n-Si solar cells ($J_0 = 1.5 \times 10^{-5}$ mA/cm^2),[21] where the band offsets promote the separation of photogenerated carriers. In Fig. 3(b), the *IQE* values were high in the wavelength λ range between 600 and 1200 nm. The λ of approximately 1200 nm is close to the band gap of Si. This means that the *IQE* spectrum was ascribed to the photogenerated carriers originating from the p-Si substrate. On the other hand, the *IQE* was negligibly small at $\lambda < 600$ nm, showing that the photogenerated holes in the 300-nm-thick n^+-$BaSi_2$ did not contribute to the photocurrent. Figures 3(c) and 3(d) are those for the n^+-$BaSi_2$ (20 nm)/p-$BaSi_2$ (500 nm)/p^+-$BaSi_2$ (50 nm) diodes. The *J*–*V* curve in Fig. 3(c) is for the sample with $p = 1 \times 10^{16}$ cm^{-3}. As shown in Fig. 3(c), leakage current was so large in the homojunction diode as expected. The *IQE* became pronounced at $\lambda < 800$ nm in Fig. 3(d), while the *IQE* was very small at $\lambda > 800$ nm because the photogenerated electrons in the p^+-Si recombined with holes before reaching the built-in field region. On the other hand, the *IQE* exceeded 30% at $\lambda = 500$ nm. Considering that the absorption length ($3/\alpha$) at $\lambda = 500$ nm is approximately 100 nm in $BaSi_2$,[12] we can state that the *IQE* spectrum in Fig. 3(d) was attributed to the photogenerated carriers originating from the p-$BaSi_2$ layer and then they were separated by the built-in electric field in the $BaSi_2$ pn junction diode. The *IQE* value distinctly increased as the p of the p-$BaSi_2$ layer decreased from 1×10^{17} to 1×10^{16} cm^{-3}, verifying the above discussion. The J_{SC} values were 1.3 and 3.6 mA/cm^2, respectively. On the basis of these results, we conclude that the operation of a $BaSi_2$ homojunction solar cell was achieved for the first time. η is as small as ~0.1% at the moment because of large leakage currents caused by defects resulting from step bunching at the p^+-$BaSi_2$/p^+-Si interface.[22] We can avoid such defects by growing a heavily doped p^+-Si epitaxial layer on a medium-doped p-Si(111) substrate instead of using a heavily doped p^+-Si substrate.

In summary, we formed n^+-$BaSi_2$ (20 nm)/p-$BaSi_2$ (500 nm)/p^+-$BaSi_2$ (50 nm) homojunction diodes on a heavily doped p^+-Si(111) ($\rho < 0.01\,\Omega$ cm) substrate and n^+-$BaSi_2$ (300 nm)/p-Si heterojunction diodes on a medium-doped p-Si(111) ($\rho > 0.1\,\Omega$ cm) substrate by MBE. The *IQE* was high at $\lambda < 800$ nm in the homojunction solar cell and exceeded 30% at $\lambda = 500$ nm, while the *IQE* was pronounced in the λ range between 600 and 1200 nm in the heterojunction solar cell. The difference in *IQE* spectrum between these solar cells clearly demonstrated the generation of photogenerated carriers in the $BaSi_2$ layer and their separation by the built-in electric field in the homojunction diode.

Acknowledgments This work was financially supported by JSPS KAKENHI Grant Numbers 15H02237 and 17K18865, and JST MIRAI. R.T. was financially supported by a Grant-in-Aid for JSPS Fellows (15J02139).

1) K. Yoshikawa, H. Kawasaki, W. Yoshida, K. Konishi, K. Nakano, T. Uto, D. Adachi, M. Kanematsu, H. Uzu, and K. Yamamoto, Nat. Energy **2**, 17032 (2017).
2) W. Shockley and H. J. Queisser, J. Appl. Phys. **32**, 510 (1961).
3) P. Jackson, D. Hariskos, R. Wuerz, O. Kiowski, A. Bauer, T. M. Friedlmeier, and M. Powalla, Phys. Status Solidi: Rapid Res. Lett. **9**, 28 (2015).
4) P. Jackson, R. Wuerz, D. Hariskos, E. Lotter, W. Witte, and M. Powalla, Phys. Status Solidi: Rapid Res. Lett. **10**, 583 (2016).
5) X. Wu, Sol. Energy **77**, 803 (2004).
6) J. Burschka, N. Pellet, S. J. Moon, R. Humphry-Baker, P. Gao, M. K. Nazeeruddin, and M. Grätzel, Nature **499**, 316 (2013).
7) W. S. Yang, J. H. Noh, N. J. Jeon, Y. C. Kim, S. Ryu, J. Seo, and S. I. Seok, Science **348**, 1234 (2015).
8) J. Evers, G. Oehlinger, and A. Weiss, Angew. Chem., Int. Ed. **16**, 659 (1977).
9) M. Imai and T. Hirano, J. Alloys Compd. **224**, 111 (1995).
10) K. Morita, Y. Inomata, and T. Suemasu, Thin Solid Films **508**, 363 (2006).
11) D. B. Migas, V. L. Shaposhnikov, and V. E. Borisenko, Phys. Status Solidi B **244**, 2611 (2007).
12) K. Toh, T. Saito, and T. Suemasu, Jpn. J. Appl. Phys. **50**, 068001 (2011).
13) M. Kumar, N. Umezawa, and M. Imai, Appl. Phys. Express **7**, 071203 (2014).
14) M. Baba, M. Kohyama, and T. Suemasu, J. Appl. Phys. **120**, 085311 (2016).
15) K. O. Hara, N. Usami, K. Toh, M. Baba, K. Toko, and T. Suemasu, J. Appl. Phys. **112**, 083108 (2012).
16) K. O. Hara, N. Usami, K. Nakamura, R. Takabe, M. Baba, K. Toko, and T. Suemasu, Appl. Phys. Express **6**, 112302 (2013).
17) R. A. McKee and F. J. Walker, Appl. Phys. Lett. **63**, 2818 (1993).
18) K. Morita, M. Kobayashi, and T. Suemasu, Jpn. J. Appl. Phys. **45**, L390 (2006).
19) Y. Imai and A. Watanabe, Intermetallics **18**, 1432 (2010).
20) D. Tsukahara, S. Yachi, H. Takeuchi, R. Takabe, W. Du, M. Baba, Y. Li, K. Toko, N. Usami, and T. Suemasu, Appl. Phys. Lett. **108**, 152101 (2016).
21) S. Yachi, R. Takabe, H. Takeuchi, K. Toko, and T. Suemasu, Appl. Phys. Lett. **109**, 072103 (2016).
22) Y. Yamashita, S. Yachi, R. Takabe, T. Sato, M. Emha Bayu, K. Toko, and T. Suemasu, Jpn. J. Appl. Phys. **57**, 025501 (2018).
23) K. Kodama, R. Takabe, S. Yachi, K. Toko, and T. Suemasu, Jpn. J. Appl. Phys. **57**, 031202 (2018).
24) Y. Inomata, T. Nakamura, T. Suemasu, and F. Hasegawa, Jpn. J. Appl. Phys. **43**, L478 (2004).
25) M. Kobayashi, Y. Matsumoto, Y. Ichikawa, D. Tsukada, and T. Suemasu, Appl. Phys. Express **1**, 051403 (2008).
26) R. Takabe, H. Takeuchi, W. Du, K. Ito, K. Toko, S. Ueda, A. Kimura, and T. Suemasu, J. Appl. Phys. **119**, 165304 (2016).
27) R. Takabe, S. Yachi, W. Du, D. Tsukahara, H. Takeuchi, K. Toko, and T. Suemasu, AIP Adv. **6**, 085107 (2016).
28) T. Suemasu, K. Morita, M. Kobayashi, M. Saida, and M. Sasaki, Jpn. J. Appl. Phys. **45**, L519 (2006).
29) R. Varache, C. Leendertz, M. E. Gueunier-Farret, J. Haschke, D. Muñoz, and L. Korte, Sol. Energy Mater. Sol. Cells **141**, 14 (2015).
30) A. N. Nesmeyanov, *Vapor Pressure of the Chemical Elements* (Elsevier, Amsterdam, 1963).
31) R. Takabe, T. Deng, K. Kodama, Y. Yamashita, T. Sato, K. Toko, and T. Suemasu, J. Appl. Phys. **123**, 045703 (2018).
32) M. Kumar, N. Umezawa, W. Zou, and M. Imai, J. Mater. Chem. A **5**, 25293 (2017).
33) J. R. Sites and P. H. Mauk, Sol. Cells **27**, 411 (1989).

© 2018 The Japan Society of Applied Physics